Piecewise-Continuous Nano-Worlds Online

P. Fraundorf[1, a)]
Physics & Astronomy/Center for Nanoscience, U. Missouri-St. Louis (63121) & Physics, Washington U. (63110), St. Louis, MO, USA

(Dated: 12 September 2016)

The familiar 1D barrier-tunneling problem, when converted to a trough-scattering problem instead, leads us to the strong-phase-object deBroglie phase-lag. This in turn reminds us of the exact Coulomb-scattering solution to the Schrödinger equation, and opens the door to real-time online electron-optic simulations with which students may discover: (a) ways to acquire and interpret data from modern multi-million dollar tools of electron-optics, (b) nano-characterization of matter on the atomic scale, (c) visualizations intermediate between direct and reciprocal space for harmonic-analysis of spatial-periodicities, and (d) important modern uses for crystal defects, including crystal surfaces themselves.

CONTENTS

I. INTRODUCTION

The one-dimensional barrier-tunneling problem is very popular in modern physics texts because it is: (a) analytically solvable, (b) connected to practical problems like alpha-decay, and (c) a beautiful illustration of the role of uncertainty in behaviors that would be classically disallowed. What is seldom mentioned, however, is that the same piecewise-constant potential setup, using a potential trough instead of a barrier, also makes contact with emerging science and technology. We show further that the exact Schrödinger-equation solution to the Coulomb-scattering problem (approximated classically by Rutherford) can similarly be inverted to reinforce this result.

In this note, in particular, we describe how that piecewise-constant potential-trough calculation gives rise to the strong-phase-object deBroglie phase-lag. We then show how calculations using this phase-lag are being used (with help from modern electronic technology) to provide students with a real-time window on the world of nano-materials, as well as on ways currently under development for exploring that world with help from high-speed electrons.

[a)] Electronic mail: pfraundorf@umsl.edu

II. THE DEBROGLIE PHASE-LAG

This is the classic one-dimensional problem: Define the vacuum wavevector $k = 2\pi/\lambda_v = \sqrt{2mU}/\hbar$ and the specimen wavevector $K = 2\pi/\lambda_s = \sqrt{2m(U-V)}/\hbar$, where U is the incident particle energy and V is potential-energy associated with our particle in the "specimen-region" e.g. of width L.

In the barrier-tunneling case $0 < U < V$, so as to make the wave classically disallowed in the specimen region. In the trough-scattering case, $V < 0 < U$ so that wave-vector (hence momentum $p = \hbar k = h/\lambda$) of our particle actually increases in the specimen-region, and therefore our particle's wavelength (e.g. in [meters per cycle]) decreases. It's not surprising then that the size of this wavelength decrease is directly related to the number of deBroglie phase cycles which take place in traversing a specimen-region of thickness L.

One can of course also calculate the various reflected and transmitted wave amplitudes (relative the amplitude incident from the left) by equating wavefunctions and wavefunction spatial 1st-derivatives at specimen-region entry and exit points. This has been done for a wide range of V/U values in Figure 1. The diagonal bands in the lower right quadrant show clearly the deBroglie phase-lag running in the negative z-direction roughly in proportion to V/U for $V < 0$.

For application to high energy ($U = 60$ to 300 [keV]) electrons, condensed-matter attractive-potentials (like work functions) are in the negative tens of Volts so that $|V/U| \ll 1$. The exact phase shift relative to $V = 0$ case is plotted (solid line) for unit-arguments in Fig. 2, along with two approximations. The first approximation (dashed) is simply the difference in wave-numbers (e.g. in [radians per meter]) times the "specimen-thickness" L, which assumes that the first order effect on the transmit-

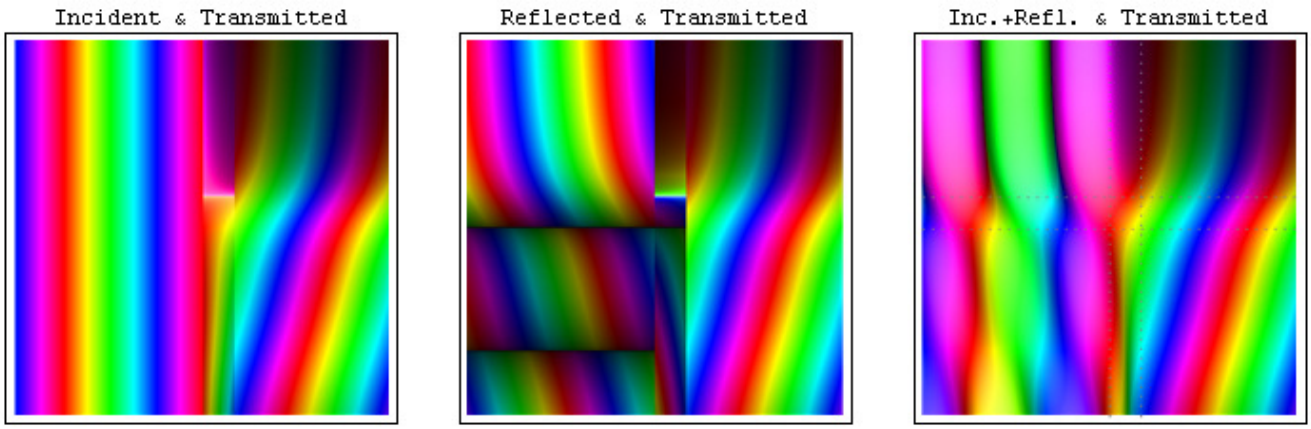

FIG. 1. One-dimensional wavefunctions (in logarithmic complex-color online) of an energy U wave incident from the left on a variable-V/U barrier/trough between $0 < z < 1$. In each of these panels, the horizontal axis runs (left to right) from $-6 \leq z \leq +6$; if we set particle mass and Planck's constant to 1, while the vertical axis shows step-potentials ranging (bottom up) from $-6 \leq V/U \leq +6$. In the rightmost panel, the dotted horizontal-band is the region of positive barrier still lower than the particle energy (transmission still classically allowed), while the dotted vertical-band marks the barrier/trough region itself.

ted phase is simply the wavelength shift during traversal.

This in turn can be Taylor-expanded around the high particle-energy U limit of $V/U \to 0$ to get the phase-shift of $\Delta\phi \simeq -(V/U)\sqrt{mU/2}L/\hbar$. This gives us the straight line (dot-dashed) in Fig. 2 which is proportional to "projected-potential" $\Phi = VL$ e.g. in [eV-m].

For a specimen-potential which varies along a beam-path in the z-direction, this might be written as $\Phi = \int_0^L V[z]dz$. This prompts us to ask, however, whether such a phase-lag (with lateral variation in x and y) will also emerge if the trough for a plane-wave flowing through a three-dimensional solid is not flat, but instead shaped like the attractive Coulomb-potential for electrons passing through a set of atomic-nuclei. Amazingly, another of the rare classical exact-solutions to the Schrdinger equation, with a potential appropriately inverted, comes to the rescue once again.

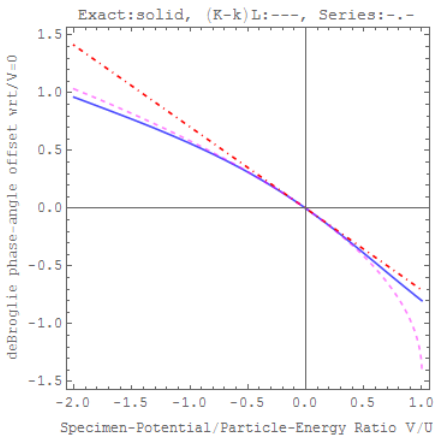

FIG. 2. Phase-shift estimates using (solid) an exact piecewise-continuous potential example, (dashed) the wavenumber-difference approximation, and (dot-dashed) the first term in the approximation's Taylor series around the $V/U \simeq 0$ or "high-energy U particle" approximation.

III. COULOMB/RUTHERFORD SCATTERING

It's often forgotten that the classical Rutherford scattering problem is connected to an exact quantum-mechanical solution to the Schrödinger equation in three-dimensions, which perhaps by accident[1] gives the same result as the classical calculation e.g. for atomic-number (Z) dependent nuclear back-scatttering. As in the case of the tunneling example discussed above, however, this problem is generally framed as a barrier-problem i.e. for predicting what happens when a positive-ion encounters a positively-charged atomic nucleus.

Once again, something also interesting emerges when we look at the "attractive" or "potential-well" version of the same calculation. As shown in Fig. 3, just as in the 1D case the interaction e.g. of an incoming electron with a localized positive charge also gives rise to a deBroglie phase-lag. Of course the Coulomb potential of atomic nuclei in condensed matter is screened at Ångström distances by the field of the electron cloud, but the principle underlying the observed phase-lag none-the-less remains that seen in our trough-scattering calculation above.

IV. ELECTRON-OPTICS SIMULATION

Thus introductory quantum-mechanics predicts an exit-surface deBroglie phase-lag, which varies depending on the projected-potential of atoms along the electron-trajectory, when an electron passes through a thin slice of condensed matter. Several issues remain, however. First,

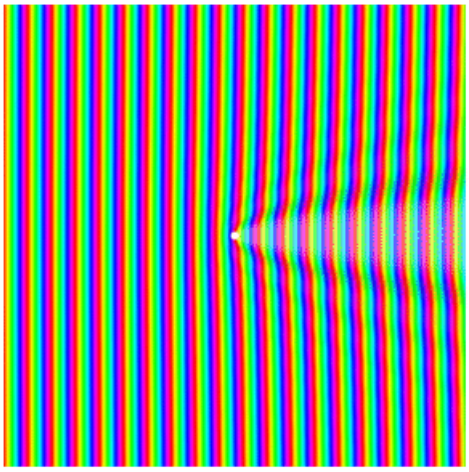

FIG. 3. Coulomb scattering (in complex-color online) of a negative charge's deBroglie extended wavefield by a fixed positive charge, from one of those rare regular solutions of the Schrödinger equation.

how can we convert that phase lag into a '"detected" map of projected-potential across the transverse coherence-width of an '"individual" electron's wave-packet! Secondly, how does this projected-potential model fare both qualitatively and quantitatively as the specimen's thickness increases?

The answers to these questions are well established in the technical literature[3–5], so we won't elaborate on them here except to illustrate the "Scherzer defocus" condition[6] (Fig. 4) for converting the phase-lag map at the exit surface into an intensity-map downstream, and then to mention two calculations that physics undergraduates might enjoy.

The "Scherzer strategy" yields useful image intensities for spatial-frequencies out to the "point-resolution maximum". It does this primarily by moving the first dark/light intensity Fourier-phase inversion away from the origin in frequency-space (the "DC-peak"), associated with "spherical-aberration transfer-function zeros" of a convex magnetic lens, until a new pair of transfer-function zeros begins to insert itself into the region between DC-peak and that first-zero.

For sufficiently thin (weak phase-object) specimens, where the deBroglie phase lag is much less than 2π, Scherzer-defocus yields intensities that are inversely proportional to projected-potential i.e. where openings between atoms are bright and columns of atoms in projection look dark. The strong phase-object (arbitrary phase-lag) analysis discussed in addition shows a subset of thickness effects, but only incompletely considers multiple scattering.

The first enjoyable calculation may be to verify that electron-phase contrast is obtained from individual electrons. Not only are electrons fermions that obey Pauli exclusion, making them unwilling to share a single coherent state like photons do in a LASER, but typical high-energy transmission-electron-microscope (TEM) specimen-currents are quite low i.e. in the nano-Ampere range.

Students might in that context use electron-energy to determine the speed of e.g. typical 100[keV] microscope electrons, and show that individual electrons in a nano-Ampere beam will be something like an inch apart in the direction of propagation. An electron-energy spread and hence energy-uncertainty at the parts-per-million level will increase the *longitudinal coherence-length'* of these electrons, but not nearly enough to allow them to overlap in the specimen even if we had a way to get them to share a common deBroglie phase. Hence on average there is only one electron traversing the specimen at a time, so all wave-interference (including diffraction effects) is being done with a single quantum-particle.

In order to map projected-potential laterally across multiple atom-columns in a condensed-matter specimen, of course, the *transverse coherence-width* of individual electrons must be expanded to many times the distance between atoms as well. This is done in modern electron-optical systems by reducing the transverse-momentum uncertainty of electrons at the specimen, largely by choice of a locally bright electron-source (like a LaB_6 or field-emission gun) to begin with.

The second calculation involves the difference in calculation-time between strong-phase-object and more-quantitative "multi-slice" image simulation. The strong-phase-object approach, as we'll see, simulates a wide range of phenomena qualitatively. For quantitative simulation, however, one must propagate the incident beam through multiple slices of the specimen.

For an $n \times n$ pixel image field this is generally done in an $n \times n$ complex-coefficient "reciprocal space". This means that each slice past the first requires that one do n^2 more strong-phase-object calculations. For a minimally useful 256×256 pixel field, this means that simulations will take some integral multiple of $65,536$ times longer, and hence be difficult to do in real time even on systems with relatively fast processors.

V. NANO-WORLDS ONLINE

The simplicity of the deBroglie phase-lag and the power of the resulting strong-phase-object approximation, combined with the speed of fast-Fourier-transform (FFT) algorithms implemented in javascript on modern processors, gives us an ability to simulate online in real-time the exploration of nanomaterials with high energy electrons. This article is not the place to detail the many types of explorations that are now possible online, in part because they make contact (beyond the worlds of electron scattering and electron optics) with condensed matter topics like: (a) crystallography and bulk/surface defect-crystallography, (b) pair and pair-pair correlations in non-crystalline materials, as well as (c) the behavior of individual molecules in the neighborhood of surfaces,

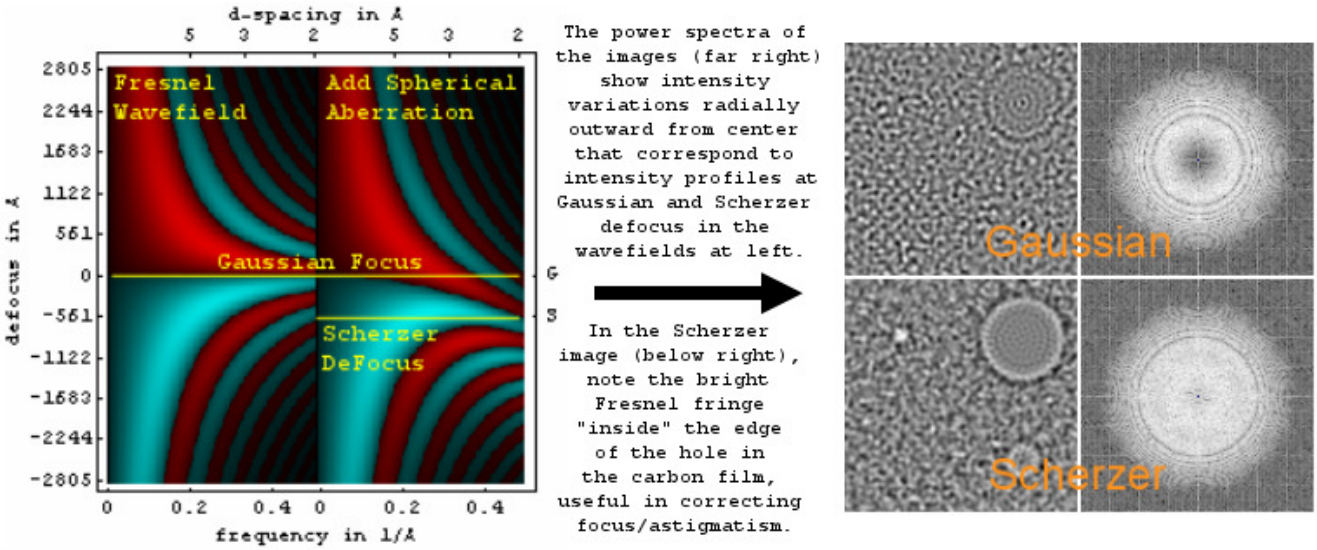

FIG. 4. Electron phase contrast transfer function and wavefield image analysis: At left find maps of contrast-transfer versus spatial-frequency without (left-half) and with (right-half) spherical aberration, as a function of imaging-system defocus in the vertical direction. At right find images (left-half) and image power-spectra (right-half) showing contrast transfer zeros at Gaussian and Scherzer defocus. In the thin-specimen limit, cyan bands (color online) in the panel at left show specimen-regions of increased projected-potential as darker, while red bands show contrast as reversed.

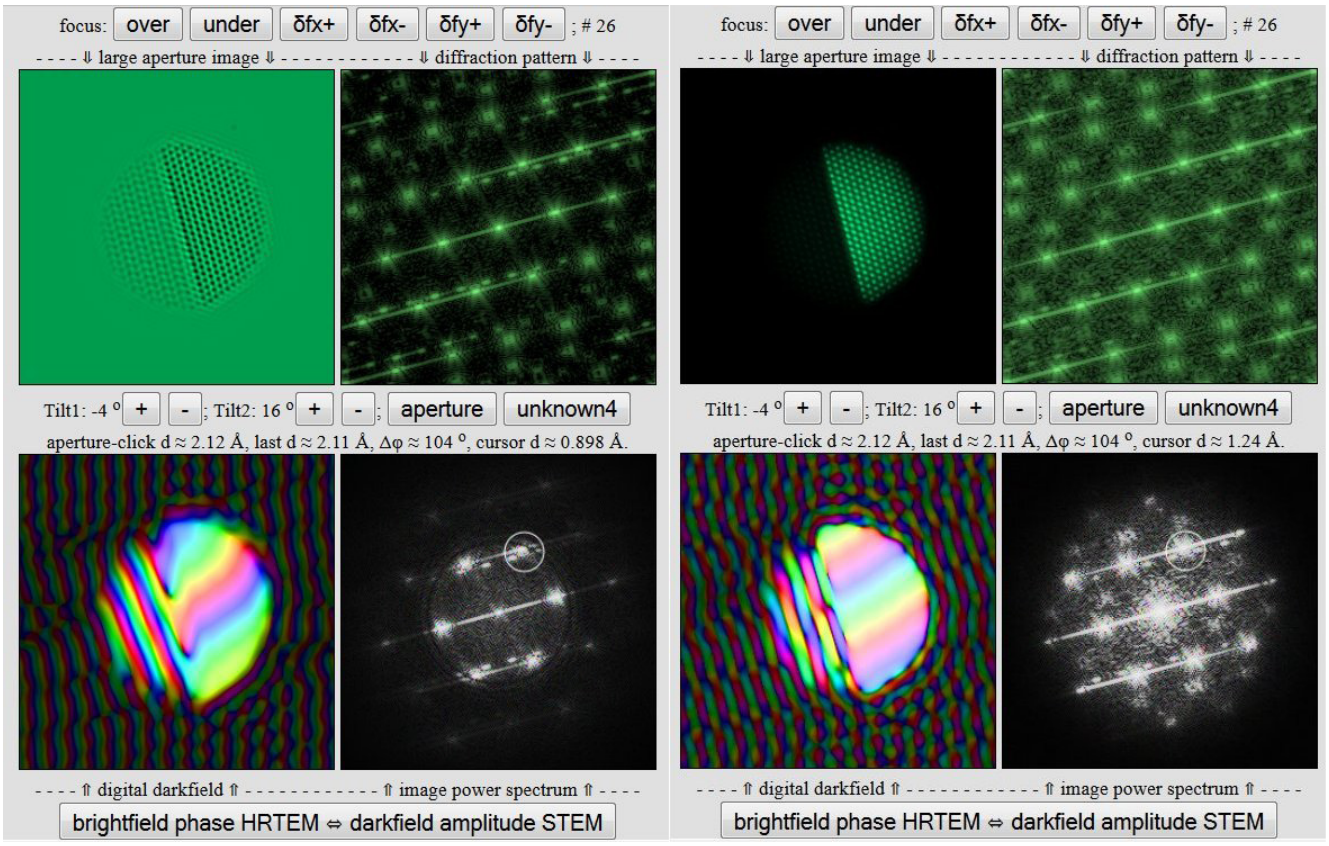

FIG. 5. Fig. 5: Brightfield high-resolution TEM (phase) and darkfield scanning-TEM (amplitude) screenshots of an "unknown" specimen in an online simulator[2], with the same defocus, orientation, and darkfield-aperture.

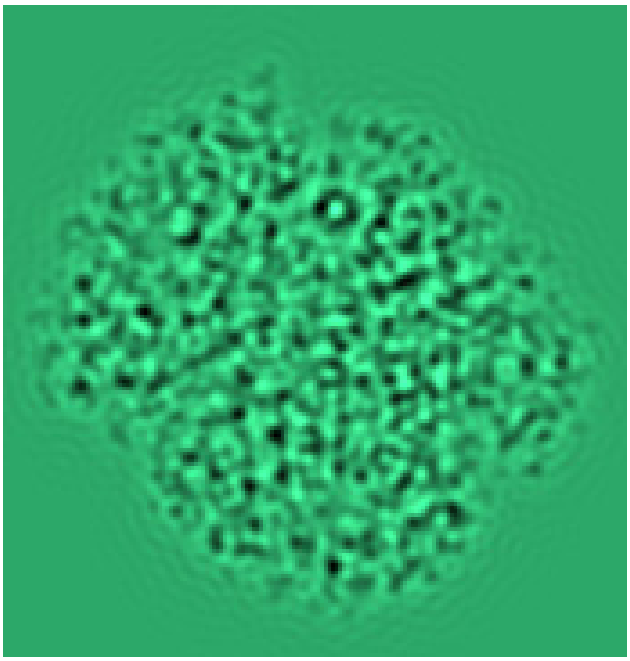

FIG. 6. A hemoglobin molecule in an online simulator, with a likely alpha-helix (circle at top) viewed end on in the absence of the vacuum re-arrangement, beam damage, and the need for a "support" that might get "in the way" experimentally.

of vacuum, of high energy electrons. Such explorations will be discussed by ourselves and others under separate cover.

However this does not make these developments irrelevant to undergraduate physics students and teachers. Far from it, since such simulators give students phenomenological access (at least qualitatively) to a wide range of phenomena, including small-wavelength (flat Ewald-sphere) diffraction from three-dimensional single and poly crystalline unknowns, strain imaging tools (including both diffraction contrast and digital darkfield interferometry), an ability to form darkfield images of selected periodicities, to switch between deBroglie phase-contrast and Z-contrast imaging modes, to get 2D "Fourier-phase information" about specimens that is impossible to obtain directly from diffraction, etc.

Figure 5, for example, shows two-screen shots of a near-Scherzer-focused online simulator examining an Au/ZnO_2 bi-crystal tilted so that the phase-interface is side-on. The left-half of the figure provides a strong-phase-object approximation deBroglie phase-contrast image of atom columns in projection down that orientation (top-left), and diffraction pattern of the crystal (top-right), a power-spectrum of the phase-contrast image (bottom-right), and the complex-color digital-darkfield image (obtained from the image Fourier transform) of periodicities selected by an aperture (white circle) in the power spectrum.

The right-half of the figure in effect reverses the path of electrons through the electron-optic system, which by reciprocity allows us to record (with comparable resolution) an incoherently-illuminated high-angle annular darkfield image of the same specimen. The physics of this type of image is somewhat different, and not the topic of this paper here. Nonetheless students and teachers can get a visceral feel for the qualitative differences between these imaging modes, whether or not they later learn to understand, and/or apply, such tools for nanoworld detective work of their own downstream.

VI. DISCUSSION

As discussed above, the piecewise-constant potential calculation used in undergraduate physics courses to explain quantum tunneling can also yield for us insight into the deBroglie phase-lag which is central to modern electron-based tools for experimental study of condensed matter. We try to make this connection here so that teachers, and textbook authors in the future, can put the connection to use.

There is also an exciting future in physics education for the kinds of electron-image simulators to which this deBroglie phase-lag connects. Students already get some visceral experience with electron-diffraction and electron-imaging as it is used today to provide insight into a wide range of condensed matter challenges in the physical and life sciences. In the latter context Fig. 6 shows what the alpha-helix in a hemoglobin molecule might look like edge-on, if we can find a way to either average over or lessen the effects of vacuum and ionization damage in real electron microscopes.

A wide range of other interesting "nano-specimens" remain yet to be assembled. In addition to specimen-tilting, future incarnations of these online simulators will allow for other imaging and analysis modes, specimen translation, and even zooming from nanometer to millimeter field-widths on procedurally-generated specimens.

Today's physics teachers and students can help apply their own skills to these developments, which mainly require access to the internet through a web-browser. In fact, these developments in turn will help with development of improved-interfaces to the modern multi-million dollar aberration-corrected instruments now available at selected facilities for researchers with interesting nanoworld puzzles to solve.

Appendix A: underlying math

In order to increase assessibility, in the main body of this paper we've tried to illustrate using quantitative graphical techniques like complex-color, which lets us show the amplitude and phase of a complex number with a single pixel. In this appendix, however, we attempt to connect interested readers to the underlying models and approximations.

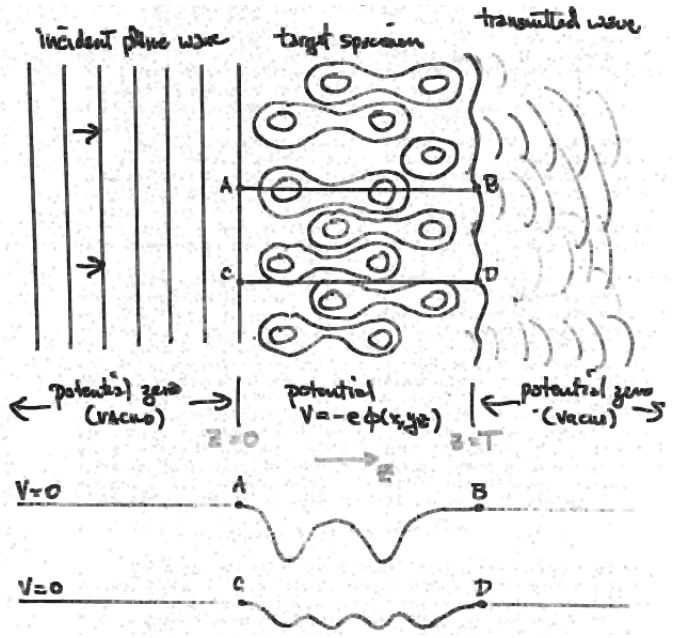

FIG. 7. Plots of electron potential $V[x, y, z]$ for electron trajectories along two different "columns" through the specimen.

1. phase-lag and projected potential

This is a standard homework exercise e.g. for modern physics, but it might not hurt to outline some details here. Consider a one-dimensional potential of the form:

$$V[z] = \begin{cases} 0 & \text{if } z < 0 \text{ (region 1: upstream)} \\ -e\Phi & \text{if } 0 \le z \le T \text{ (region 2: specimen)} \\ 0 & \text{if } z > T \text{ (region 3: downstream)} \end{cases} \tag{A1}$$

where Φ is an average *projected-potential* in the specimen column of interest. This average potential (cf. Fig. 7) depends strongly on the proximity of atomic nuclei in the specimen to the selected column, and will e.g. be much less if the column follows a *tunnel between atoms* through the structure. Our objective is to examine ways that the transmitted wave reflects changes, from column-to-column, in this projected-potential.

For incident plane waves of the form $\Psi[z,t] = Ae^{\imath(kz-\omega t)}$ in the positive z-direction with electron kinetic energy $E_r = eV_r$, write out the Schrödinger equation for regions 1, 2 and 3 with parameters specified in terms of the quantities given above. The one-dimensional non-relativistic free-particle Schrödinger wave equation, for instance, may be written:

$$-\frac{\hbar^2}{2m}\frac{\partial^2\psi}{\partial z^2} + V[z]\psi = \imath\hbar\frac{\partial\psi}{\partial t}, \tag{A2}$$

where ψ is the wave function whose amplitude squared yields a probability density as a function of position and time, the expression $\imath\hbar\partial/\partial t$ on the right is the "energy operator", and the first term on the left represents the classical kinetic-energy operator i.e. the "momentum operator" $\imath\hbar\partial/\partial z$ squared over $2m$. The Schrödinger equation basically differs from region to region here only by the addition of the negative but piecewise-constant work-function potential energy $-e\Phi$ which multiplies the wavefunction in region 2.

Next write out the form for wavefunction solutions of that equation in each of these regions, in terms of some yet undetermined constants. The high-energy electron wave in the first two regions might be described for region 1 (upstream) as $\psi_1[z] = Ae^{\imath kz} + Be^{-\imath kz}$, and for region 2 (specimen) as $\psi_1[z] = Ce^{\imath kz} + De^{-\imath kz}$. Here the "'vacuum wavevector" $k = 2\pi/\lambda_v = \sqrt{2meV_r}/\hbar$ while the "specimen wavevector" $K = 2\pi/\lambda_s = \sqrt{2me(\Phi + V_r)}/\hbar$ is larger (implying a smaller electron wavelength λ_s in the specimen) because the solid attracts electrons. We'll leave it as an exercise for the reader to do the same for region 3 (downstream), using say F and G for the forward and reverse wave coefficients in each case.

Following this, write out boundary conditions that these constants obey at the boundaries between region 1, 2, and 3. For instance at the $z = 0$ boundary between regions 1 and 2, equating ψ values gives $A + B = C + D$ while equating $\partial\psi/\partial z$ values gives $\imath k(A - B) = \imath K(C - D)$. Do the same thing then for the z=T boundary between regions 2 and 3, and then solve for the "amplitude" of the transmitted wave at $z = T$ as a function of the incident amplitude A, and wave vectors k and K in regions 1 and 2. Also show how this simplifies when $V_r \gg \Phi$. The results are discussed in the text.

At relativistic speeds, electron momentum goes from $p \simeq \sqrt{2m_eE_k}$ to $p = \sqrt{2E_k(E_o + E_k)}/c$. Here rest energy $E_o \equiv m_ec^2$, where c and m_e are lightspeed and electron rest-mass, respectively. Hence wavenumber $k = \frac{2\pi}{\lambda}$ is changed via the dependence of wavelength on momentum $\lambda = h/p$. Also, the ratio between wavelength outside the specimen to wavelength inside the specimen (i.e. the specimen's refractive index) changes subtly as well. Therefore the factor of $\frac{1}{2V_r}$, which multiplies projected potential to get the optical path difference, becomes $\frac{1}{V_r}\frac{E_o+E_k}{2E_o+E_k}$. Otherwise, the above analysis of phase shift remains intact[3,4].

2. point-charge scattering

Following e.g. Messiah's Chapter XI on the Coulomb Interaction[1], a naked-charge wavefield model may be obtained if the $1/r$ Coulomb potential term is inserted into Schrödinger's partial differential equation:

$$\left(-\frac{\hbar^2}{2m}\nabla^2 + \frac{Z_1Z_2e^2}{r}\right)\psi[\vec{r}] = E\psi[\vec{r}]. \tag{A3}$$

This is of course the hydrogen atom potential, but here we'd like the solution in a form that can be broken down into incident and scattered plane wave components. Such a solution may be expressed in terms of the three-argument confluent hypergeometric function ${}_1F_1[u|v|w]$

as:

$$\psi_c = Ae^{\imath kz}{}_1F_1\left[-\frac{\imath}{ka}\,|1|\,\imath k(r-z)\right], \qquad \text{(A4)}$$

where A is an adjustable constant and $a \equiv \hbar^2/(Z_1 Z_2 me^2)$ is inversely proportional to the interaction strength. This wave function is the one that is plotted in Fig. 3.

The above differential equation might be modified for addition of a neutralizing charge sphere at radius R, by merely stepping the potential for $r > R$ down to zero. Solutions for no potential of course generally look something like $Ae^{\imath kz}$. Since the solutions for both potentials in standalone form are known, one might take the next step with a composite wave model for the neutralized charge by simply joining those two solutions up at the spherical $r = R$ boundary.

Spherically-symmetric atomic-scattering-factors are often used instead to propagate a planar (or convergent/divergent) wavefront though the specimen. For quantitative work, multislice strategies[5] consider the sequential evolution of a scattered wave through atomically thin slices of specimen in sequence.

Regardless, to first order the electron wavefunction (whose transverse coherence is many atoms in width) will exhibit a deBroglie phase-shift (relative to nearby columns) which is from section A 1 proportional to the projected-potential at the exit surface of the specimen. The problem is that an image of the phase-contrast in the exit wave-function cannot be detected directly, and so in the next section we turn to electron optics for a solution to that problem.

For sufficiently thick specimens and/or with incoherent illumination, atomic columns will also exhibit an amplitude decrease due to scattering which is a monotone increasing-function of projected potential. Given the projected-potential this too is relatively easy to approximate roughly.

3. electron-optics phase/amplitude contrast

Scattering in quantum mechanics results in an electron wave which is both phase shifted, and changed in direction. A classic use of the Born approximation, the WKB method, and partial wave analyses has been calculating the angular dependence of scattering from single atoms, based on the details of charge distribution within – Rutherford's famous discovery of the nucleus was an early consequence thereof. Fortunately for the electrons discussed here, these angular issues are less important because scattering angles are well under 10 milliradians.

If one uses apertures which are large enough to include both scattered and unscattered beams (e.g. in the back focal plane of the objective lens, where exit surface waves are separated according to direction rather than amplitude), then one can imagine imaging the amplitude-added unscattered and scattered wavefields together (at least over specimen distances less than the transverse coherence width of incident electrons). Hence the first practical requirements for electron phase contrast imaging are thin specimens, moderate coherence width illumination, and large objective apertures.

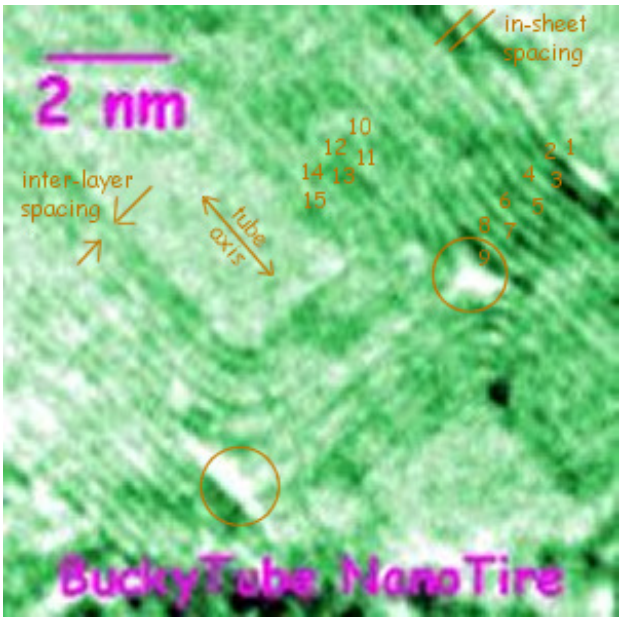

FIG. 8. An electron phase contrast image of the internal structure of a 15 wall carbon nanotube, the innermost 6 atomic layers of which form an internal closure.

Under these conditions, the imaged exit surface wave from a thin crystal looks like the incident wave, multiplied by $e^{+i\sigma}$, where $\sigma[x,y] \simeq \frac{k}{2V_r}\Phi[x,y]$ varies with lateral coordinate values x and y across the specimen. If the phase angle is small (i.e. much less than π), the multiplying factor can be approximated by $e^{+i\sigma} \simeq 1+i\sigma$.

Imagine a one dimensional specimen with only spatial frequency $q = 1/\Lambda$, where Λ is the repeat distance, e.g. so that $\sigma[x] = \sigma_o cos[2\pi qx]$. At the exit surface, the wavefield will have been multiplied by $\psi[x] = 1+i\sigma_o cos[2\pi qx]$. Note that, as long as $\sigma_o << 1$, the amplitude of the composite wave field is hardly affected by the specimen's periodicity. In light microscopy, this problem is overcome by inserting a Zernike phase plate[4] for shifting the scattered beam only by an additional $\pi/2$, resulting (when recombined) in first order amplitude effects.

In the absence of a suitable phase plate, one can instead defocus one's imaging optics so as to sample the wavefield downstream (or virtually, upstream as well) from the exit surface of the specimen, at a point where phase differences at the exit surface interfere with one another to create ripples in intensity which may be photographed. What defocus setting is appropriate depends on the spatial frequencies of interest.

Physically, the scattered wavefield evolves by convolution with the Fresnel propagator, which is oft written (apart from a constant factor[3]) as $e^{\frac{i\pi(x^2+y^2)}{\lambda\Delta z}}$. Here Δz is

the distance from the exit-surface along the beam direction, or the "defocus setting", defined so as to be positive in the downstream (underfocus) direction. In frequency space, this is equivalent to multiplying the wavefield by the propagator's Fourier transform, the transfer function e^{-iW} defined here in terms of the "defocus function" $W[\Delta z] = \pi\lambda\Delta z(q_x^2 + q_y^2)$. For our single frequency specimen, the imaged amplitude is thus modulated by $\psi = 1 + ie^{-iW}\sigma_o cos[2\pi qx]$. The intensity found in the image becomes $I \equiv \psi^*\psi = 1 + 2sin[W]\sigma_o cos[2\pi qx]$.

The factor $sin[W]$, a function of both defocus Δz and spatial frequency q, thus determines both the strength and sign of intensity ripples corresponding to specimen structure, in the captured image. It predicts dark spots in the neighborhood of large phase shifts (e.g. atom columns), for example when W is near $-\pi/2$. We also might want to choose defocus Δz so that the images are simplest to interpret, e.g. so that $sin[W]$ is finite and constant for as wide a range of frequencies as possible. To assist with this, we've plotted $sin[W]$ as a function of transverse spatial frequency q, and defocus Δz, for unit wavelength on the left hand side of Figure 4.

Spherical aberration in the objective lens also affects the image. The effect is shown graphically on the right hand side of Figure 4. Since zeros in $sin[W]$ correspond to phase reversals for the corresponding periodicity, a traditional goal has been to select a defocus for which these zero's are moved outward to as high a frequency as possible. As illustrated in the diagram, Scherzer defocus is the setting of choice in this regard.

Recent work has concentrated on focussed-probe illumination in which the aberrations occur upstream of the specimen, which probe in "scanning transmission" (STEM) is rastered across the specimen, resulting generally in more amplitude rather than phase contrast, and on "aberration-correction" which uses controllable aberrations to correct uncorrectable aberrations (like spherical) in one focus plane only. The latter requires more work in focusing, but has allowed sub-Angstrom lateral resolutions, even at beam voltages which are below the knock-on threshold from important light atoms like carbon[7].

For quantitative microscopy of thicker specimens in real microscopes, of course, other issues must be considered as well: e.g. vibration and electrical instabilities, knowledge of specimen thickness, astigmatism, and the range of illumination angles in the beam. Even then the theory remains quite elegant, and except for the effects of specimen thickness can be visualized by changes in the fingerprint of Fig 4.

Of course, this analysis might seem abstract. Au contraire! Recall that amorphous materials in projection are, unlike crystals, likely to show a uniform distribution of periodicities. As a result, the zeros of the imaginary part of the Fresnel transfer function, for the current defocus setting in the right side of Fig 4, show up as rings in the power spectrum from amorphous material *in every HREM image.*

ACKNOWLEDGMENTS

Thanks to industry and university collaborators across the region for related projects.

[1] A. Messiah, *Quantum Mechanics*, Vol. Vol. I (John Wiley and Sons, 1958).

[2] P. Fraundorf, S. Wedekind, T. Savage, and D. Osborn, "Single-slice nanoworlds online," Microscopy and Microanalysis **22:S3**, 1442–1443 (2016).

[3] J. C. H. Spence, *Experimental high-resolution electron microscopy*, 2nd ed. (Oxford University Press, 1988).

[4] L. Reimer, *Transmission electron microscopy: Physics of image formation and microanalysis*, 4th ed. (Springer Science, NY, 1997).

[5] E. J. Kirkland, *Advanced Computing in Electron Microscopy*, 2nd ed. (Plenum Press, NY, 2010).

[6] O. Scherzer, "The theoretical resolution limit of the electron microscope," J. Appl. Phys. **20**, 20–29 (1949).

[7] O. L. Krivanek, M. F. Chisholm, V. Nicolosi, T. J. Pennycook, G. J. Corbin, N. Dellby, M. F. Murfitt, C. S. Own, Z. S. Szilagyi, M. P. Oxley, S. T. Pantelides, and S. J. Pennycook, "Atom-by-atom structural and chemical analysis by annular dark-field electron microscopy," Nature **464**, 571–574 (2010).